Colloids and Surfaces A: Physicochem. Eng. Aspects 481 (2015) 600–608

Contents lists available at ScienceDirect

Colloids and Surfaces A: Physicochemical and Engineering Aspects

journal homepage: www.elsevier.com/locate/colsurfa

Dynamic contact angle of dilute polymer solution drops impacting on a hydrophobic surface

V. Bertola [a,*], M. Wang [b]

[a] School of Engineering, University of Liverpool, Brownlow Hill, Liverpool L69 3GH, UK
[b] Department of Engineering Mechanics and CNMM, Tsinghua University, Beijing 100084, China

HIGHLIGHTS

- Systematic measurements of the apparent dynamic contact angle of dilute polymer solution drops are presented.
- Polymer concentrations cover almost entirely the dilute regime.
- Drop impacts onto commercial PTFE surfaces are investigated at different Weber numbers.

GRAPHICAL ABSTRACT

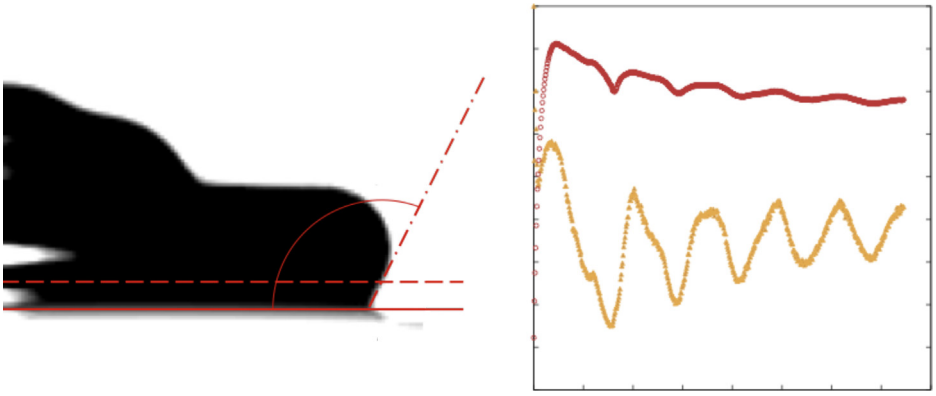

ARTICLE INFO

Article history:
Received 22 April 2015
Received in revised form 16 May 2015
Accepted 19 May 2015
Available online 25 June 2015

Keywords:
Dynamic contact angle
Drop impact
Dilute polymer solutions

ABSTRACT

The dynamic contact angle of dilute polymer solution drops impacting on a hydrophobic PTFE surface is studied experimentally by high-speed imaging, for polymer concentrations ranging between 0 ppm and 400 ppm, and impact Weber numbers between 15 and 115. Images with spatial resolution of 16.4 μm/pixel were captured at 8000 fps to resolve the short time-scale dynamics. Results show that the receding contact angle of dilute polymer solution drops is significantly smaller than in case of drops of pure water, suggesting that the receding contact line encounter a higher resistance to its displacement. The minimum contact angle decreases with respect to both increasing polymer concentration and increasing Weber number. At lower Weber numbers, contact angle oscillations were observed, which can be related to the liquid flow to and from the rim during drop retraction.

© 2015 Elsevier B.V. All rights reserved.

1. Introduction

The equilibrium shape of a drop deposited on a surface is generally described using the well-known Young-Laplace equation with respect to the interfacial tensions between the solid and the liquid, γ_{SL}, the solid and the vapour, γ_{SV}, and the liquid and the vapour, γ:

$$\gamma_{SL} + \gamma\cos\theta_{eq} = \gamma_{SV} \quad (1)$$

where θ_{eq} is the thermodynamic equilibrium contact angle between the drop and the surface [1,2].

If the drop moves parallel to the surface, however, one can observe an advancing (θ_A) and a receding contact angle (θ_R), respectively at the leading edge and at the trailing edge. This implies an

* Corresponding author.
E-mail address: Volfango.Bertola@liverpool.ac.uk (V. Bertola).

http://dx.doi.org/10.1016/j.colsurfa.2015.05.052
0927-7757/© 2015 Elsevier B.V. All rights reserved.

Table 1
Fluid properties.

	0 ppm	50 ppm	100 ppm	200 ppm	300 ppm	400 ppm
$\rho_{20\,^\circ C}$, kg/m^3	1000	1000	1000	1000	1000	1000
$\mu_{20\,^\circ C}$, mPa s	1	1.058	1.115	1.23	1.345	1.46
$\sigma_{20\,^\circ C}$, mN/m	72	70	70	70	70	70
$\tau_{20\,^\circ C}$, ms	-	15.31	21.65	30.62	37.51	43.31

adhesion force, which can be described either by using Furmidge's equation [3,4]

$$F = \gamma D(\cos\theta_R - \cos\theta_A) \tag{2}$$

where D is the drop base diameter perpendicular to the contact angle plane, or by introducing the concept of line tension [5]:

$$F = \gamma \frac{D}{2}(\cos\theta - \cos\theta_{eq}) \tag{3}$$

where θ is the apparent (observed) contact angle. A comparative analysis of these two approaches can be found in [6]. Different approaches must be used in case of chemically heterogeneous [7,8] or rough surfaces [9,10], and in case of non-circular drops [11].

An important case where advancing and receding contact angles are observed is drop impact. When a liquid droplet impacts onto a solid surface, it spreads radially taking the shape of a disk (often referred to as "lamella"), eventually surrounded by a toroidal rim. During this stage, the impact kinetic energy is partly converted into surface energy, and partly lost because of viscous dissipation. After reaching maximum spreading, i.e. when nothing is left of the initial kinetic energy, the lamella initiates retracting under the action of capillary forces, in order to minimise surface energy. During the expansion and retraction stages one can observe respectively an advancing and a receding contact angle, which in turn allow the definition of a contact angle hysteresis around the point of maximum spreading.

Whilst the open literature reports several experimental and theoretical studies about the dynamic contact angle of Newtonian drops [12–18], many applications involve the use of complex fluids, such as polymer or surfactant solutions, which exhibit a wetting dynamics remarkably different from the case of simple liquids. Even in the case of very dilute solutions, comparison with the Newtonian solvent (e.g., water) reveals significant differences in the behaviour of the moving contact line during the spreading and/or receding phase, in the amplitude of the dynamic contact angle, as well as in the intrinsic time of the phenomenon [19–21]. A well-known example is the so-called anti-rebound effect of polymer additives: When a droplet of water falls on to a hydrophobic surface, such as the waxy leaf of a plant, the drop is often observed to bounce off, however the addition of very small quantities (~100 ppm) of a flexible polymer can completely prevent rebound, by reducing the recoil velocity of the drop after the inertial spreading of two orders of magnitude [22,23]. This apparently surprising phenomenon (since the shear viscosity and surface tension of such drops are almost identical to those of pure water), is intimately related to the contact angle dynamics, as initially suggested by comparison with drop impact experiments where wetting was artificially reduced or removed [24,25].

Despite their scientific and industrial importance, to date there is a lack of dynamic contact angle data for non-Newtonian drops in the open literature [19]. The present work contributes to address this gap through systematic dynamic contact angle measurements of polymer solution drops impacting on a hydrophobic surface of commercial interest (PTFE), for different impact velocities and polymer concentrations that cover the entire dilute regime.

2. Materials and methods

2.1. Fluids characterisation

The fluids considered in the present work are dilute solutions of polyethylene oxide (PEO) in de-ionized water. The PEO, supplied by Aldrich Chemicals under the form of granular powder, has average molecular weight M_w = 4000 kDa, and typical density of 1210 kg/m^3. In dilute solutions, the average distance among polymer molecules is larger than their size, so that their interactions are negligible: polymers exhibit a random coil conformation and can be described as spherical particles suspended in the solvent. For a critical value of concentration (the overlap concentration) polymer chains become randomly entangled, which corresponds to a marked increase in the polymer solution viscosity. The overlap concentration can be calculated as:

$$c^\circ = \frac{1}{[\eta]_0} \tag{4}$$

where $[\eta]_0$ is the characteristic viscosity, which for a PEO solution is related to the molecular weight as [26]:

$$[\eta]_0 = 0.0125 M_w^{0.78} \tag{5}$$

Thus, for the solutions considered in the present work the overlap concentration is 567 ppm. To investigate the fluid in the dilute regime, one master solution was prepared with a mass concentration of 400 ppm, which was then diluted to obtain solutions at 300, 200, 100 and 50 ppm. Polymer solutions were prepared from a same batch of polymer, protected from direct illumination and from heat sources, and used within 2–3 weeks.

Viscosities were measured by means of a rotational rheometer (Haake MARS II) equipped with a 60 mm plate/plate geometry and Peltier temperature controller, while equilibrium surface tensions were measured using a maximum bubble pressure instrument (Krüss PocketDyne). Finally, the relaxation time was calculated as a function of the characteristic viscosity, concentration, and temperature using the empirical formula [27]:

$$\tau = (1.82 \times 10^{-3}[\eta]_0 - 2.9 \times 10^{-11}[\eta]_0^3 - 0.51)\sqrt{c}\exp(-0.0004T^2) \tag{6}$$

Table 1 summarizes the properties of fluids and drops considered in these experiments. Note that while viscosity is approximately a linear function of the polymer concentration in the dilute regime, the surface tension does not change because PEO saturates the free surface already at low concentrations.

2.2. Experimental setup and procedure

Drops were generated using a syringe with blunt hypodermic needle (gauge 21, 0.495 mm i.d.) driven by a micrometric screw, and detached under their own weight. The characteristic drop diameter calculated from drop weight measurements, $D_0 = (6\,m/\pi r)^{1/3}$, where m is the drop mass, and ρ the water density, was 3.09 ± 0.1 mm for water drops and 2.93 ± 0.1 mm for polymer solution drops; thus, the drop equilibrium radius, $D_0/2$, is smaller

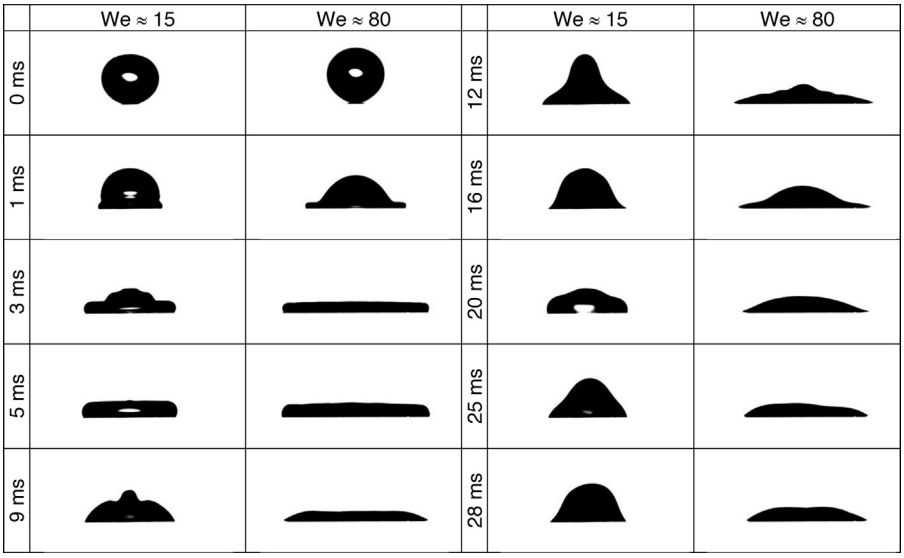

Fig. 1. Side views of 200 ppm PEO solutions during the first stages of impact on a PTFE surface, at different Weber numbers.

than the capillary length, $a = (\sigma/\rho g)^{1/2}$, where σ is the surface tension (2.48 mm for water and 2.39 mm for the polymer solutions), so that surface forces prevail ensuring that the equilibrium shape of drops is spherical.

The dispensing needle was suspended above a glass slide coated with a PTFE film (equilibrium contact angle for water: $118.7^\circ \pm 1.7^\circ$). The drop release height was adjusted using a Vernier height gauge at 2, 6, 10, and 14 cm, to obtain theoretical free-fall velocities, $v = \sqrt{2g(H - D_0)}$ of 0.58, 1.06, 1.38 and 1.64 m/s, respectively; in this range, the theoretical free fall velocity is almost identical to the actual impact velocity measured from digital images [25]. Thus, the corresponding Weber numbers, $We = \rho v^2 D_0/\sigma$, characterising the competition between inertia and surface forces, covered approximately the range between 15 and 115.

A high-frame rate CMOS camera (Phantom v9000) equipped with a zoom lens (Edmund Optics VZi400) and horizontally aligned with the surface recorded the impacts of single drops. Back-to-front illumination was provided by a LED backlight (Philips AccentLed) which ensured a uniform illumination intensity, and images with a resolution of 576×286 pixels were captured at 8000 frames per second. Magnification was kept constant throughout all experiments and lengths on the image could be calculated by comparison with a reference length (spatial resolution: 16.4 μm/pixel). To ensure a fine optical alignment, the camera, the heated surface and the backlight were fixed to an optical breadboard. All experiments were repeated five times for the sake of statistical analysis.

2.3. Contact angle measurement

Apparent contact angles can be measured from side views of sessile or impacting drops using several different methods, among which the best-known is the Axisymmetric Drop Shape Analysis method (ADSA) [28–30], where a solution of the Laplace equation is fitted to the drop shape by minimising the error between the theoretical and observed drop boundaries, or simplified versions using circles instead of Laplace curves [31,32]. However, methods based on the ADSA concept require the drop symmetry, which significantly reduces their applicability. Alternative approaches consist in fitting polynomials to find the drop boundary only in a region near the contact line [33], possibly enhancing the drop boundary detection with sub-pixel resolution [34], or using piecewise continuous polynomial functions (B-splines) [35,36].

Whilst these methods can calculate, more or less accurately, the contact angles of drops at equilibrium and of drops in weak non-equilibrium conditions, such as drops moving on an inclined surface, they are not suitable whenever drops are strongly out of equilibrium, for example during the impact on a solid surface. In fact, during impact the drop shape undergoes large, rapid, and sometimes non-symmetric deformations, and apparent contact angles cover almost the entire range between 0° and 180°, therefore it is almost impossible to fit with sufficient accuracy the drop shape, or a part of it, in every image of the sequence describing the impact. In these cases, methods to measure the contact angle based on direct image processing, i.e., without edge fitting, are preferable.

Recently, advanced techniques based on the local edge contour and on the image intensity gradient analysis were proposed [37,38]; unlike edge fitting approaches, these techniques are less sensitive to the image resolution. A simpler method, and the one used in the present work, is to approximate the local tangent with a line interpolating the three-phase-point and the nearest point of intersection between the drop contour and a horizontal line parallel to the baseline (i.e., a secant), as shown schematically in Fig. 2. Despite its simplicity, this method proves accurate in comparison with other image-processing algorithms, with the advantage of a minimum computational cost.

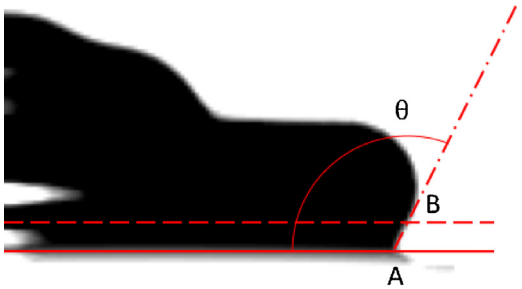

Fig. 2. Schematic of the contact angle measurement procedure. The tangent line to the drop profile in the contact point is approximated with the secant passing through the contact point (A) and the point defined by the drop profile and the dashed line parallel to the baseline (B).

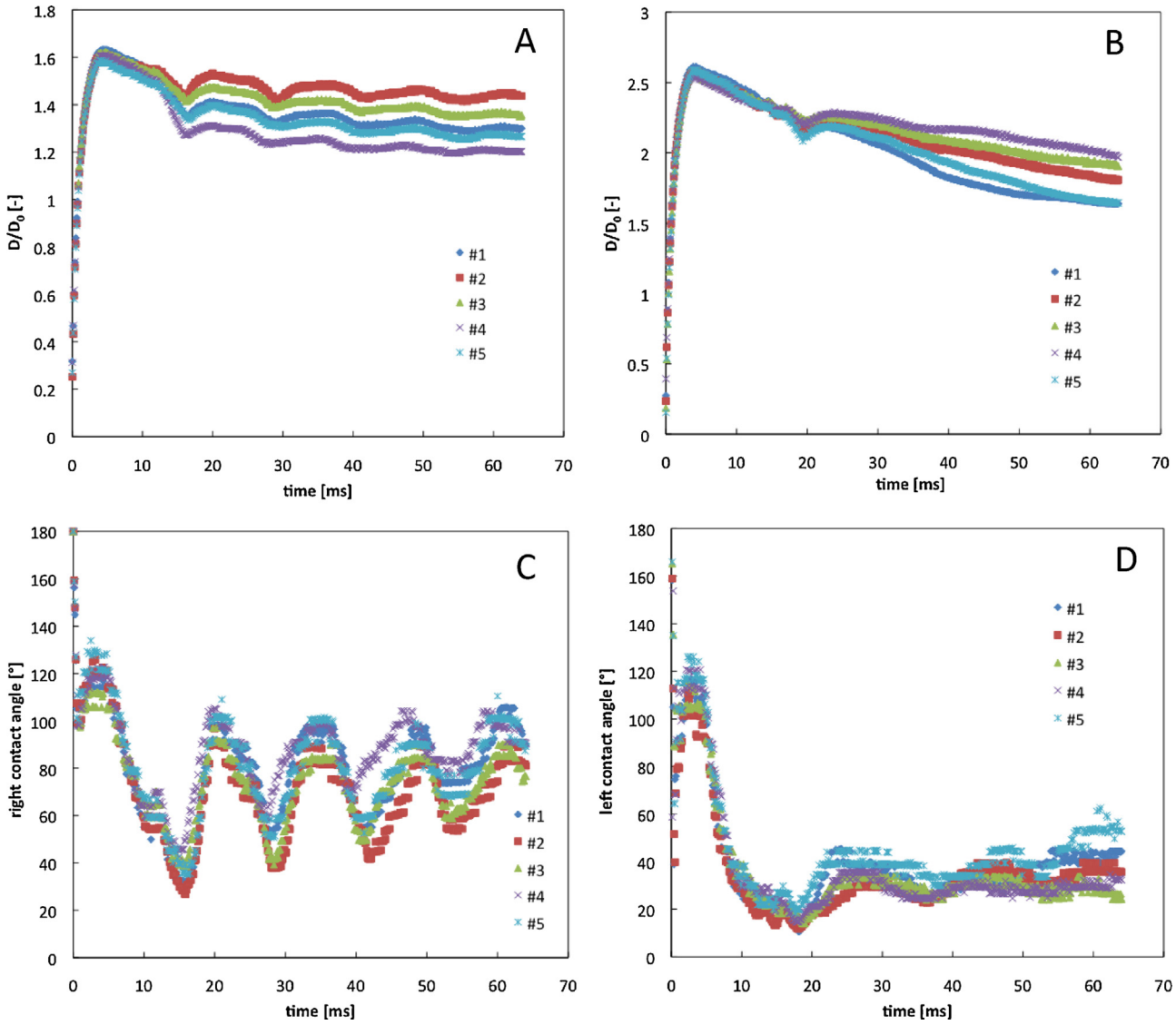

Fig. 3. Repeatability of base diameter (A, B) and contact angle (C, D) measurements based on the comparison of five individual time series, for We ≈ 15 (A, C) and We ≈ 80 (B, D); c = 200 ppm.

3. Results

Examples of image sequences from side views of impacting drops, displayed in Fig. 1, provide a qualitative understanding of the contact angle dynamics during the expansion and retraction stages of impact, and highlight the differences between drops of polymer solution and drops of pure water. As observed previously, such differences are negligible during the expansion stage, but significant during retraction; in particular, the retraction of polymer solution drops occurs in a much longer time, and is characterised by a peculiar stick-slip behaviour of the contact line, which can be associated to regular oscillations of the contact angle.

The repeatability of contact angle and base diameter measurements can be analysed from the comparison of experimental time series obtained under the same conditions (polymer concentration and impact Weber number). Fig. 3 displays examples of contact angle and base diameter time series, where each graph shows the results measured for five identical drops at two different Weber numbers. Both water and polymer solution drop impacts can be reproduced very accurately, especially during the inertial expansion stage and the initial stage of retraction, corresponding to the first contact angle oscillation, irrespective of the Weber number; as drops continue to oscillate on the surface, one can observe a progressive increase of the measurement standard deviation, which however remains within ±10% of the mean value in all cases. It must be remarked that the repeatability analysis shown in Fig. 3 concerns homogeneous sets of experiments, i.e., with identical experimental parameters, and carried out in a short period of time (of the order of 10–15 min); when different sets of experiments are considered, at least one parameter changes (e.g., the Weber number, or the polymer concentration), therefore errors are not directly comparable, in principle.

Figs. 4 and 5 compare the average dimensionless diameter and apparent contact angle of drops containing different concentrations of polymer during the first 80 ms after impact, for two Weber numbers (We ≈ 15 and We ≈ 80), respectively. In both cases, the inertia-dominated spreading is almost identical for all solutions, however there is a clear difference between the retraction dynamics of water drops and that of any polymer solution; whilst water drops exhibit a fast recoil, eventually leading to full or partial rebound after about 40 ms, where $D/D_0 \rightarrow 0$, and limited dynamic hysteresis between the advancing and receding contact angles,

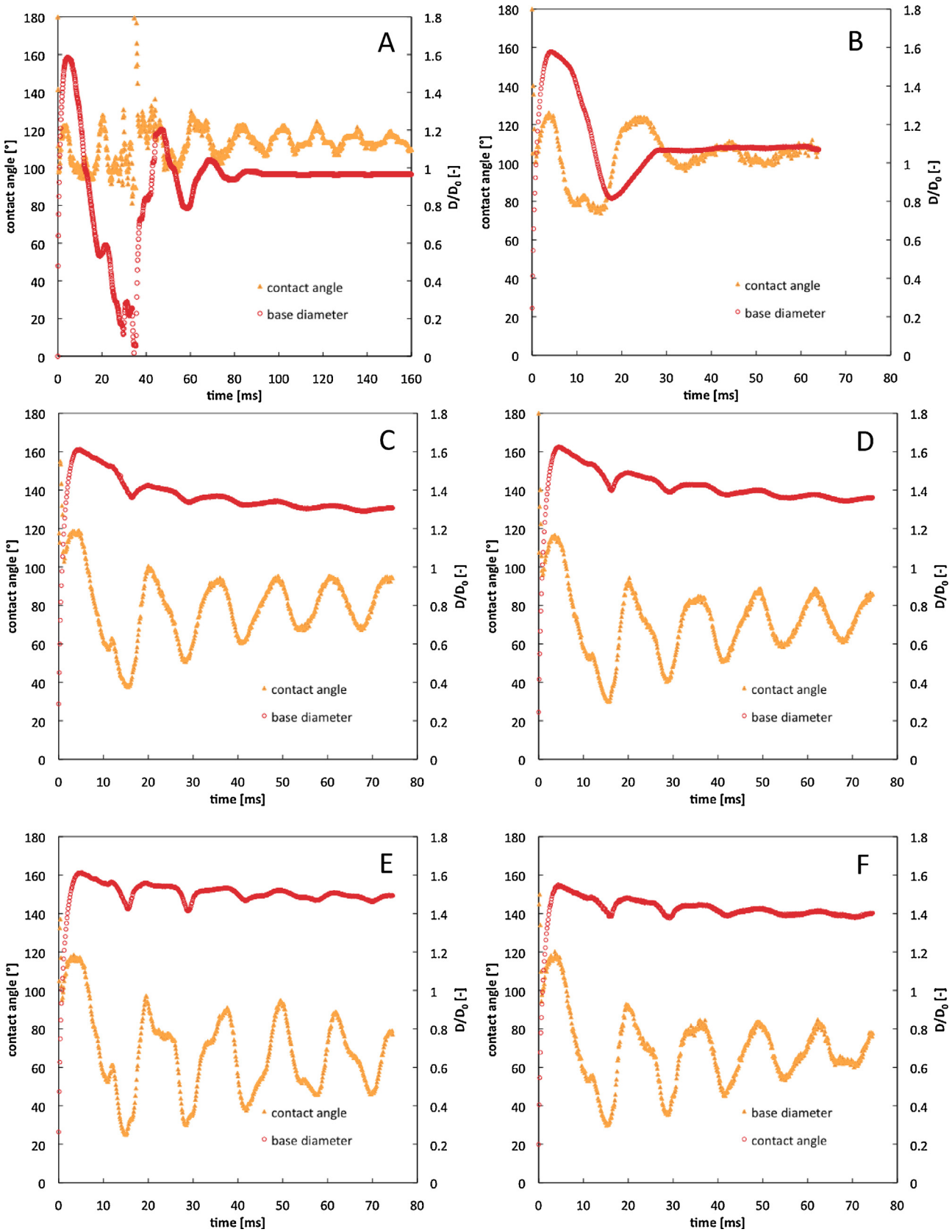

Fig. 4. Drop base diameter (O) and average apparent contact angle (△) during the impact and retraction of drops (We ≈ 15); (A) water; (B) c = 50 ppm; (C) c = 100 ppm; (D) c = 200 ppm; (E) c = 300 ppm; (F) c = 400 ppm.

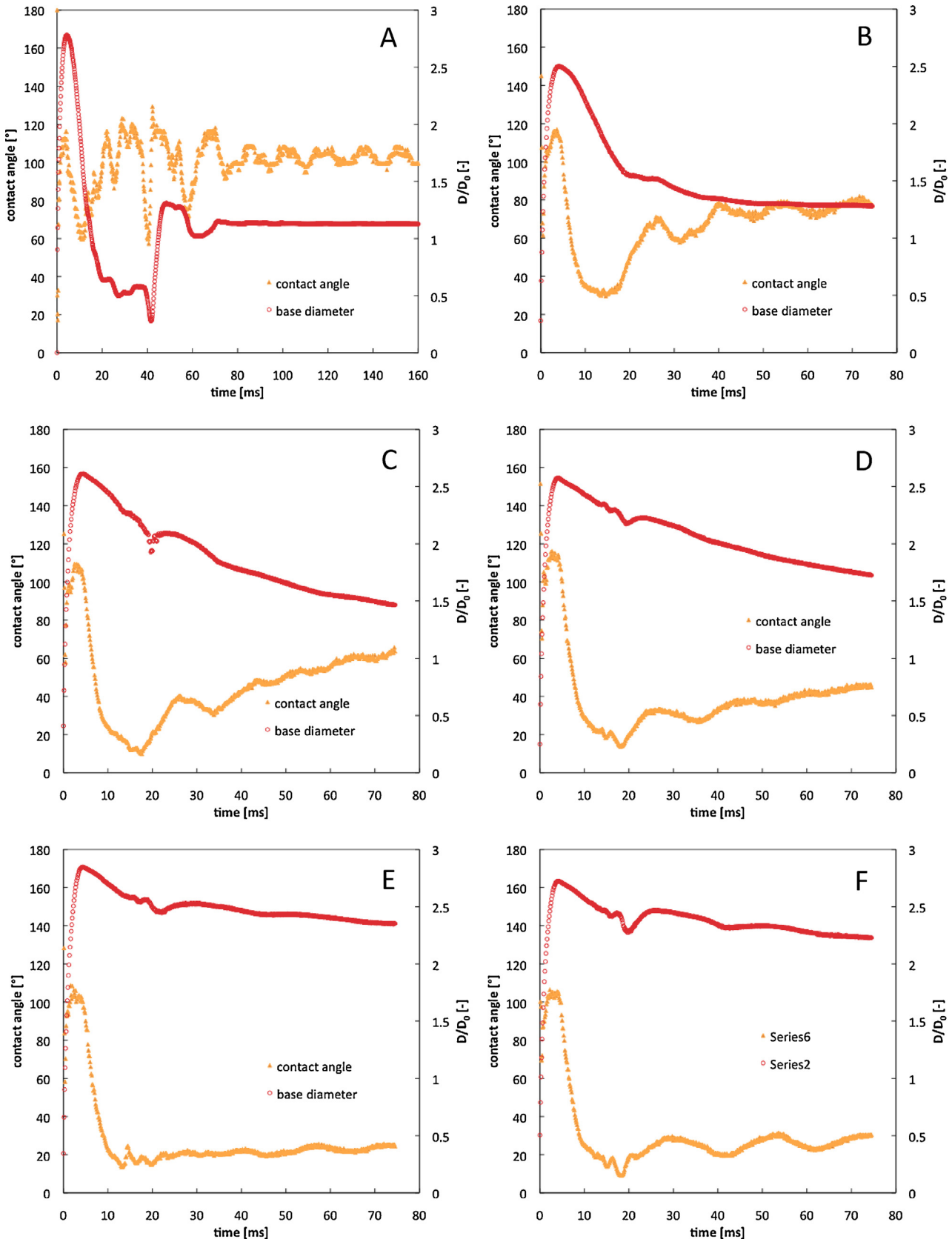

Fig. 5. Drop base diameter (O) and average apparent contact angle (△) during the impact and retraction of drops (We ≈ 80); (A) water; (B) c = 50 ppm; (C) c = 100 ppm; (D) c = 200 ppm; (E) c = 300 ppm; (F) c = 400 ppm.

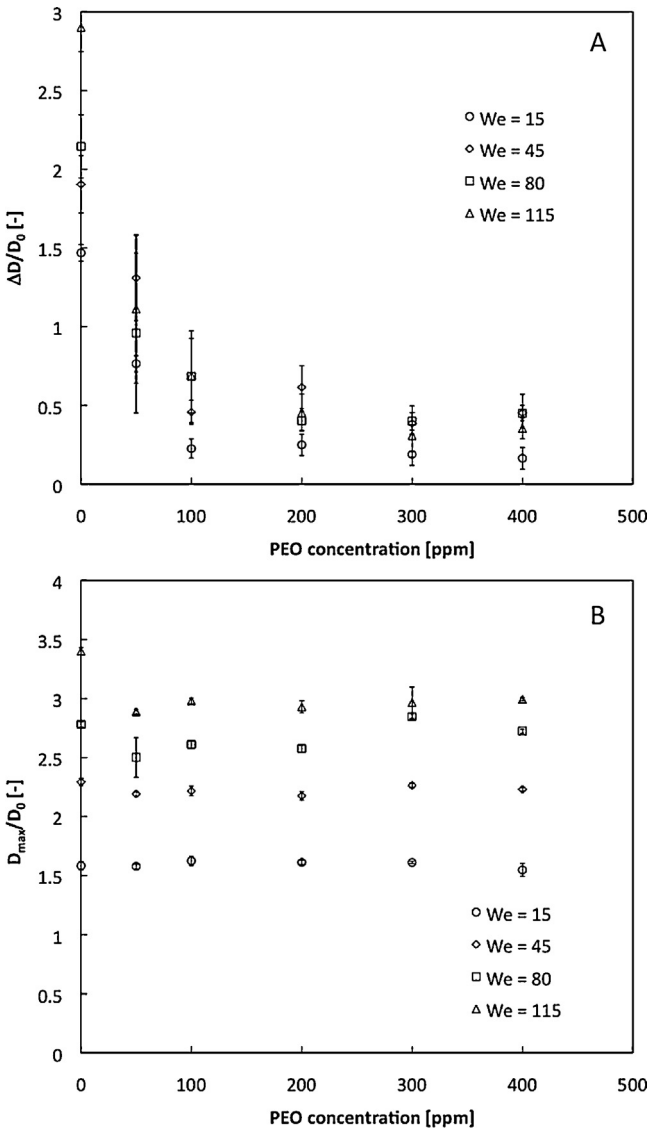

Fig. 6. Slip length during the first oscillations (A) and maximum spreading diameter (B).

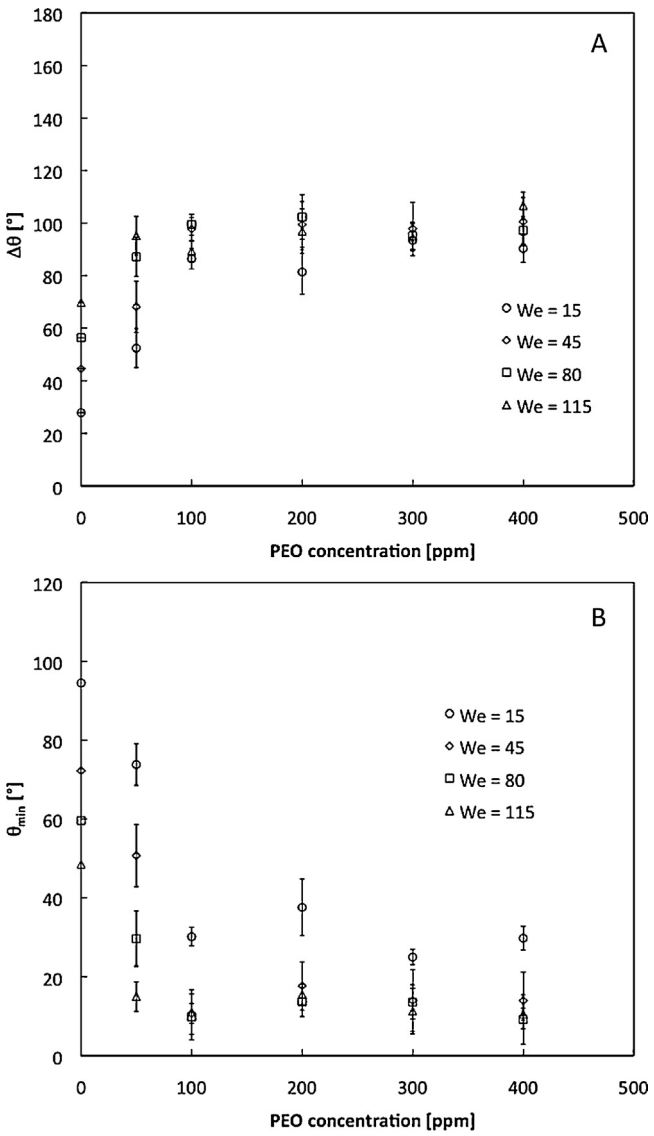

Fig. 7. Contact angle hysteresis during the first oscillations (A) and minimum contact angle (B).

polymer solution drops have a slow retraction dynamics, characterised by ample oscillations of the apparent contact angle. These oscillations are associated with a peculiar stick-slip behaviour of the contact line, which has a sharp acceleration in the direction of retraction followed by a quick expansion, generating a series of local minima in the base diameter time series; the local minima of the base diameter, i.e., the points where the contact line velocity changes its sign, correspond to the local minima of the apparent contact angle. Such behaviour becomes weaker at higher Weber numbers, where the base diameter decreases monotonically with only one stick-slip event corresponding to the absolute minimum of the apparent contact angle.

The analysis of data in Figs. 4 and 5, together with the drop side views displayed in Fig. 1, suggest the stick-slip behaviour of the contact line can be associated to a pinning/depinning of the contact line, where pinning should be interpreted as "lower contact line velocity" and depinning as "higher contact line velocity"; in addition, the apparent contact angle seems to be affected significantly by the drop deformation due to the liquid flow from the rim towards the centre of the lamella, and vice-versa during the oscillating retraction stage. The relative importance of inertial effects of the bulk fluid flow can be estimated by the Reynolds number, $\mathrm{Re} = \rho u_r D_0/\mu$, where u_r is the fluid velocity; previous studies [39] have shown that the fluid velocity of a 200 ppm PEO solution drop during retraction, measured on a horizontal plane at a distance of 10 μm from the impact surface, is of the order of 250 mm/s (i.e. two orders of magnitude larger than the contact line velocity), so that using the fluid properties in Table 1 it yields Reynolds numbers between 500 and 700. Thus, the apparent dynamic contact angle cannot be predicted by models based on a fluid dynamic approach [40,41], which require small Capillary and Reynolds numbers; from a different point of view, one can observe that the timescale of contact angle oscillations, $(\mathrm{d}\theta/\mathrm{d}t)^{-1}$, or that of the bulk fluid flow during retraction, D_0/u_r, are much shorter than the timescale to complete drop retraction.

Fig. 6 displays the amplitude of the first oscillation of the base diameter, $\Delta D = D_{max} - D_{min}$ (Fig. 6a), and the maximum base diameter (Fig. 6b), as a function of the polymer concentration in the solution. The amplitude of the first oscillation decreases monotonically increasing the polymer concentration, however significant changes are observed only for $c < 100$ ppm. The maximum spreading diameter is approximately constant for all polymer solutions,

and is only slightly larger for drops of pure water, because of the smaller viscosity.

The dynamic contact angle hysteresis during the first oscillation, i.e., the difference between the first relative maximum and the first relative minimum, $\Delta\theta$, is shown in Fig. 7a. This quantity grows up to a polymer concentration of 100 ppm, and then remains approximately constant at higher concentrations; its dependence on the Weber number is noticeable only for zero or small polymer concentrations, and becomes negligible above 100 ppm. It must be remarked these values are significantly different from the contact angle hysteresis measured in quasi-static conditions (e.g., by slowly changing the volume of a sessile droplet), which in case of water on a PTFE surface is $22.8^\circ \pm 2.9^\circ$. Fig. 7b shows values of the minimum contact angle (i.e., the first relative minimum), which is related to the contact line force at the beginning of retraction, but is also partly determined by the inertial displacement of the liquid in the rim. This quantity decreases with respect to the polymer concentration, which corresponds to an increase of the horizontal component of the surface force that drives retraction; this suggests that the surface force must overcome a larger resistance in order to displace the contact line, in agreement with previous studies on a similar system [20,21]. These results are also confirmed by forced dewetting experiments of dilute polymer solution drops, where the contact line velocity was controlled by removing the fluid with a syringe pump [42], although a direct comparison is not possible.

4. Conclusions

The impact dynamics and the apparent dynamic contact angle of dilute polymer solution drops impacting on a hydrophobic PTFE surface are significantly different from those observed in drops of pure water under the same experimental conditions. In particular, the retraction dynamics after the inertial spreading stage exhibits a peculiar stick-slip behaviour, which becomes less pronounced at higher impact Weber numbers, and is related to contact angle oscillations. The amplitudes of the slip length and of the contact angle oscillations scale with the polymer concentration.

The minimum apparent contact angle of polymer solution drops at the beginning of retraction is very small in comparison with water drops, and decreases when the polymer concentration is increased; this suggests the receding movement of the contact line encounters a higher resistance due to the polymer molecules, confirming previous studies.

Results suggest the value of the dynamic contact angle is the result of three independent contributions: dynamic wetting (e.g., Cox's hydrodynamic approach), the inertial displacement of the liquid in the rim (which is neglected in current dynamic wetting models because of the longer time scales), and the excess line tension that builds up when polymer chains stretch as they are swept by the receding contact line.

Acknowledgements

V.B. gratefully acknowledges support from the Collaborative Program for Distinguished Overseas Scholar of Tsinghua University (Grant No. 201208300004) and the Tsinghua University Initiative Scientific Research Program (No. 2014z22074).

References

[1] P.-G. de Gennes, Wetting: statics and dynamics, Rev. Modern Phys. 57 (1985) 827–863.
[2] T. Young, An Essay on the Cohesion of Fluids, Philosophical Transactions of the Royal Society of London 95, 1805, pp. 65.
[3] C.G.L. Furmidge, Studies at phase interfaces. I. The sliding of liquid drops on solid surfaces and a theory for spray retention, J. Colloid Sci. 17 (1962) 309–324.
[4] E.B. Dussan, On the ability of drops or bubbles to stick to non-horizontal surfaces of solids. Part 2. Small drops or bubbles having contact angles of arbitrary size, J. Fluid Mech. 151 (1985) 1–20.
[5] J.W. Gibbs, On the Equilibrium of Heterogeneous Substances, Transactions of the Connecticut Academy of Arts and Sciences, 1876.
[6] R. Tadmor, Approaches in wetting phenomena, Soft Matter 7 (2011) 1577–1580.
[7] A. Friedman, Wetting and adsorption at chemically heterogeneous surfaces, in: Mathematics in Industrial Problems, The IMA Volumes in Mathematics and its Applications 57, Springer, New York, 1994, pp. 185–197.
[8] P.S. Swain, R. Lipowsky, Contact angles on heterogeneous surfaces: a new look at Cassie's and Wenzel's laws, Langmuir 14 (1998) 6772–6780.
[9] E. Bormashenko, Wetting transitions on biomimetic surfaces, Phil. Trans. R. Soc. A 368 (2010) 4695–4711.
[10] E. Bormashenko, Y. Bormashenko, G. Oleg, On the nature of the friction between nonstick droplets and solid substrates, Langmuir 26 (2010) 12479.
[11] S.F. Chini, V. Bertola, A. Amirfazli, A methodology to determine the adhesion forces of arbitrarily shaped drops with convex contact lines, Colloids Surf. A: Physicochem. Eng. Aspects 436 (2013) 425–433.
[12] T. Jiang, S. Oh, J.C. Slattery, Correlation for dynamic contact angle, J. Colloid Interface Sci. 69 (1979) 74–77.
[13] M. Bracke, F.D. Voeght, P. Joos, The kinematics of wetting: the dynamic contact angle, Prog. Colloid Polym. Sci. 79 (1989) 142–149.
[14] J. Fukai, Y. Shiiba, T. Yamamoto, O. Miyatake, D. Poulikakos, C.M. Megaridis, Z. Zhao, Wetting effects on the spreading of a liquid droplet colliding with a flat surface: experiment and modeling, Phys. Fluids 7 (1995) 236–247.
[15] H.-Y. Kim, J.-H. Chun, The recoiling of liquid droplets upon collision with solid surfaces, Phys. Fluids 13 (2001) 643–659.
[16] S. Sikalo, C. Tropea, E.N. Ganic, Dynamic wetting angle of a spreading droplet, Exp. Therm. Fluid Sci. 29 (2005) 795–802.
[17] I.S. Bayer, C.M. Megaridis, Contact angle dynamics in droplets impacting on flat surfaces with different wetting characteristics, J. Fluid Mech. 558 (2006) 415–449.
[18] I.V. Roisman, L. Opfer, C. Tropea, M. Raessi, J. Mostaghimi, S. Chandra, Drop impact onto a dry surface: role of the dynamic contact angle, Colloids Surf. A: Physicochem. Eng. Aspects 332 (2008) 183–191.
[19] V. Bertola, Effect of polymer additives on the apparent dynamic contact angle of impacting drops, Colloids Surf. A: Physicochem. Eng. Aspects 363 (2010) 135–140.
[20] M.I. Smith, V. Bertola, Effect of polymer additives on the wetting of impacting droplets, Phys. Rev. Lett. 104 (2010) 154502.
[21] V. Bertola, Dynamic wetting of dilute polymer solutions: the case of impacting droplets, Adv. Colloids Interfaces 193–194 (2013) 1–11.
[22] R. Crooks, D.V. Boger, Influence of fluid elasticity on drops impacting on dry surfaces, J. Rheol. 44 (2000) 973–996.
[23] V. Bergeron, D. Queíreí, Water droplets make an impact, Phys. World 14 (5) (2001) 27–31.
[24] A. Rozhkov, B. Prunet-Foch, M. Vignes-Adler, Impact of drops of polymer solutions on small targets, Phys. Fluids 15 (7) (2003) 2006–2019.
[25] V. Bertola, An experimental study of bouncing Leidenfrost drops: comparison between Newtonian and viscoelastic liquids, Int. J. Heat Mass Transfer 52 (2009) 1786–1793.
[26] F.E. Beiley, J.V. Koleske, Poly(ethylene oxide), Academic Press, New York, 1976.
[27] V.N. Kalashnikov, A.N. Askarov, Relaxation time of elastic stresses in liquids with small additions of soluble polymers of high molecular weights, J. Eng. Phys. Thermophys. 57 (1989) 874–878.
[28] Y. Rotenberg, L. Boruvka, A.W. Neumann, Determination of surface tension and contact angle from the shapes of axisymmetric fluid interfaces, J. Colloid Interface Sci. 93 (1983) 169–183.
[29] O.I. del Rio, A.W. Neumann, Axisymmetric drop shape analysis: computational methods for the measurement of interfacial properties from the shape and dimensions of pendant and sessile drops, J. Colloid Interface Sci. 196 (1997) 136–147.
[30] M. Hoorfar, A.W. Neumann, Recent progress in axisymmetric drop shape analysis (ADSA), Adv. Colloid Interface Sci. 121 (2006) 25–49.
[31] L. Li, W. Kang, D. Ye, A contact angle measurement method for the droplets in EWOD-based chips, in: Proc. 2nd IEEE, Conf. Nano/Micro Eng. Molec. Sys., Bangkok, Thailand, 2007, 16th–19th January.
[32] J. Goclawski, W. Urbaniak-Domagala, The method of solid–liquid contact angle measurement using the images of sessile drops with shadows on substratum, in: Proc. Memstech Lviv-Polyana, Ukraine, 2007, pp. 135–140, 23rd–26th May.
[33] E. Atefi, J. Adin Mann, H. Tavana, A robust polynomial fitting approach for contact angle measurements, Langmuir 29 (2013) 5677–5688.
[34] S.F. Chini, A. Amirfazli, A method for measuring contact angle of a symmetric and symmetric drops, Colloids Surf. A: Physicochem. Eng. Asp. 388 (2011) 29–37.
[35] A.F. Stalder, G. Kulik, D. Sage, L. Barbieri, P. Hoffmann, A snake-based approach to accurate determination of both contact points and contact angles, Colloids Surf. A 286 (2006) 92–103.
[36] C. Xu, J.L. Prince, Snakes, shapes, and gradient vector flow, IEEE Trans. Image Process. 7 (1998) 359–369.
[37] D. Biolè, V. Bertola, A goniometric mask to measure contact angles from digital images of liquid drops, Colloids Surf. A: Physicochem. Eng. Aspects 467 (2015) 149–156.

[38] D. Biolè, V. Bertola, The fuzzy interface of drops, Comput. Visual. Sci. (2015), http://dx.doi.org/10.1007/s00791-015-0244-0
[39] M.I. Smith, V. Bertola, Particle velocimetry inside newtonian and non-newtonian droplets impacting a hydrophobic surface, Exp. Fluids 50 (2011) 1385–1391.
[40] R.G. Cox, The dynamics of the spreading of liquids on a solid surface. Part 1. Viscous flow, J. Fluid Mech. 168 (1986) 169–194.
[41] E.B.V. Dussan, On the spreading of liquids on solid surfaces: static and dynamic contact lines, Ann. Rev. Fluid Mech. 11 (1979) 371–400.
[42] M.I. Smith, J.S. Sharp, Origin of contact line forces during the retraction of dilute polymer solution drops, Langmuir 30 (2014) 5455–5459.